ACS APPLIED MATERIALS & INTERFACES

Research Article

www.acsami.org

Biomimetic and Cell-Mediated Mineralization of Hydroxyapatite by Carrageenan Functionalized Graphene Oxide

Hongyan Liu,[†,‡] Ju Cheng,[§] Fengjuan Chen,[†,‡] Fengping Hou,[†,‡] Decheng Bai,[§] Pinxian Xi,*[,†,‡] and Zhengzhi Zeng*[,†,‡]

[†]Key Laboratory of Nonferrous Metal Chemistry and Resources Utilization of Gansu Province, State Key Laboratory of Applied Organic Chemistry, College of Chemistry and Chemical Engineering, [‡]The Research Center of Biomedical Nanotechnology, and [§]Key Lab of Preclinical Study for New Drugs of Gansu Province, School of Basic Medical Sciences, Lanzhou University, Lanzhou 730000, P. R. China

Supporting Information

ABSTRACT: In bone tissue engineering, it is imperative to design multifunctional biomaterials that can induce and assemble bonelike apatite that is close to natural bone. In this study, graphene oxide (GO) was functionalized by carrageenan. The resulting GO-carrageenan (GO-Car) composite was further used as a substrate for biomimetic and cell-mediated mineralization of hydroxyapatite (HA). It was confirmed that carrageenan on the GO surface facilitated the nucleation of HA. The observation of the effect of the GO-Car on the adhesion, morphology, and proliferation of MC3T3-E1 cells was investigated. In vitro studies clearly show the effectiveness of GO-Car in promoting HA mineralization and cell differentiation. The results of this study suggested that the GO-Car hybrid will be a promising material for bone regeneration and implantation.

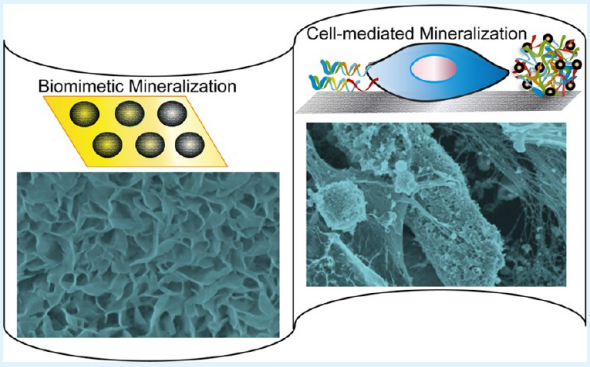

KEYWORDS: *graphene oxide, carrageenan, hydroxyapatite, Biomimetic mineralization, cell-mediated*

1. INTRODUCTION

Tissue engineering is an attractive interdisciplinary field that combines the basic principles and techniques of material science, biology, and manufacturing to fabricate various substitutes for regenerating damaged tissues and organs.[1−5] Bone tissue engineering is an important strategy for the repair or replacement of bone through the combination of scaffolds, implanted cells, and biologically active molecules.[6,7] The study of structure−function relationships in bone tissue engineering has been promoted the development of bioactive substitutes and engineered biomaterials. As the major component of natural bone, hydroxyapatite ($Ca_{10}(PO_4)_6(OH)_2$, exhibits excellent biocompatibility and bioactivity,[8] and it has been widely used in bone replacement systems.[9] However, compared to natural bone, HA exhibits poor tensile strength and fracture toughness, which limited the practical applications. A number of other materials have been integrated with HA to improve the mechanical property, such as polymer,[10] alumina (Al_2O_3),[11] zirconia, silicon carbide,[12] titanium (Ti), or Ti alloys.[13,14] It is well-known that the nature bone is composed of HA together with collagen fibrils and proteins in the extracellular matrix.[7] However, the process is unclear.[15] The possible mechanism is due to the mechanical signals provided by the self-assembled collagen[16] and the presence of the charged proteins, which facilitate the mineralization of HA.[7,17,18] Therefore, the design of biointerfaces, through which natural components can be readily integrated into diverse synthetic biomaterials, remains as a key challenge in tissue engineering.

To develop the ideal interface for biomimetic mineralization, an effective strategy is to explore organic/inorganic composite that can mimic the nature of bone. Carrageenan is naturally linear polysaccharides of about 25 000 galactose derivatives, consisting of highly sulfated alternating 3-linked-β-D-galactopyranose and 4-linked-R-D-galactopyranose units.[19] It exhibits very good biocompatibility and has been widely used in the food, pharmaceutical, and cosmetic industries.[20] Because of the abundant sulfate groups, carrageenan has the potential to mimic the charged proteins present in the extracellular matrix. For the inorganic materials, they should exhibit good biocompatibility as well as mechanical properties. Graphene, the basic building block for naturally occurring graphite, has attracted tremendous attention because of its low cost, unique structure, and extraordinary electronic and mechanical properties.[21,22] However, the intrinsic van der Waals interactions between layers of graphene easily results in agglomeration, which leads to insolubility, inevitably affecting the dispersion of graphene before implementation of graphene-based nanocomposites. In the family of graphene materials, GO is viewed

Received: July 28, 2013
Accepted: February 14, 2014
Published: February 14, 2014

   dx.doi.org/10.1021/am4057826 | ACS Appl. Mater. Interfaces 2014, 6, 3132−3140

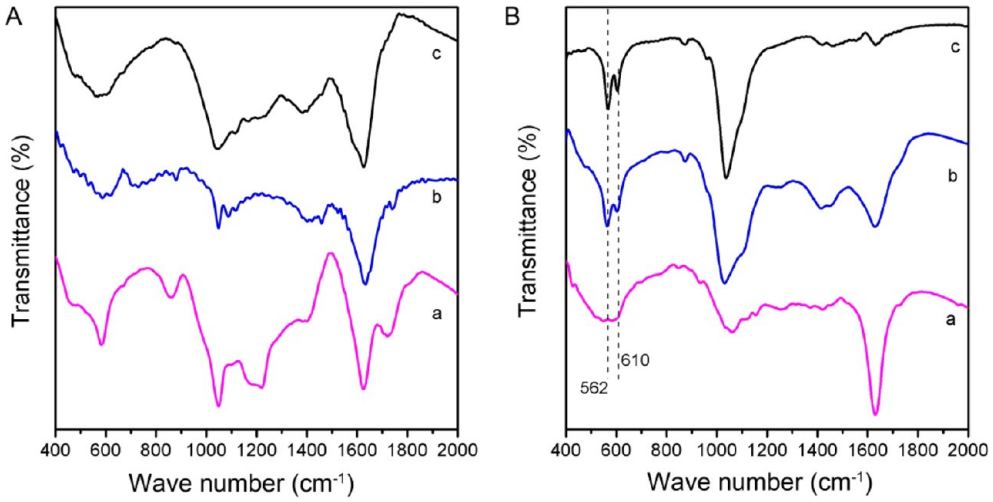

Figure 1. FTIR spectra of (A) GO and (B) GO-Car (a) before and (b, c) after being incubated for (b) 7 and (c) 14 days.

as an amphiphile with a largely hydrophobic basal plane and hydrophilic edges.[23] The oxygen-containing functional groups of GO not only are able to greatly improve the dispersibility of GO in aqueous solution but also can serve as anchor sites for binding with metal ions or nanoparticles.[24,25] More importantly, GO possesses a high mechanical strength and induces no obvious toxic effects in vivo[26,27] It is also worth noting that GO has been utilized along with gelatin, chitosan, and other polymers that were reported to show a significant increase in tensile strength and Young's modulus.[28−31] GO offers distinct advantage, it has emerged as an attractive precursor to be functionalized for biomimetic synthesis of materials for bone replacement.

In this study, we choose to use carrageenan to functionalize GO and investigate the HA precipitation on it. The surface modification of GO by carrageenan resulted in a bioinspired surface with sulfate groups, which further proved to facilitate the binding of calcium ions and thus provide a lot nucleation points for HA nucleation. The biocompatibility of the GO-Car composite was evaluated. Various cellular activities and mineralization were observed on the GO-Car surfaces. The cells on the GO-Car surface exhibit higher activities. Finally, we confirmed that the functionalization of carrageenan on the GO surface can cause increased cell mineralization.

2. EXPERIMENTAL SECTION

Materials. Graphite (500 meshes) was obtained from Acros Organic Company. Carrageenan was obtained from Alfa Aesar. Other reagents and solvents were purchased from Guangfu Chemical Co. (Tianjin, China). For cell culture, the mouse MC3T3-E1 preosteoblast cell line was obtained from the Chinese Academy of Medical Sciences (China). Fetal bovine serum (FBS) was obtained from Si ji qin Co. (China). Calcium- and magnesium-free phosphate buffered saline (PBS) and trypsin were obtained from Invitrogen (USA) and Dulbecco's modified eagle medium (DMEM) was obtained from Thermo Fisher Scientific Inc. (USA). Dimethyl sulfoxide (DMSO) and 25% glutaraldehyde were purchased from Beijing Chemical Plant (Beijing, China). β-Glycerol phosphate was purchased from Sigma-Aldrich Co. (USA).

Preparation of GO-Car and Biomimetic Mineralization of Hydroxyapatite. GO was made using established procedures.[32] 30 min sonication of GO in water makes a aqueous dispersion of GO (20 mL of a 1 mg mL^{-1} solution). The GO suspension was then mixed with an aqueous solution of carrageenan (1 mg mL^{-1}) and stirring for 12 h. Product was collected by centrifugation (8,000 rpm), washed with water, and redispersed in water.

The GO and GO-Car substrate were prepared according to a procedure reported.[33] Glass substrates were cleaned and dried. After 3-amino-propyl-triethoxysilane (APTES) treatment, GO and GO-Car were immobilized on the APTES-treated substrate by immersing the substrates in GO or GO-Car aqueous suspension (5 mg mL^{-1}) for 12 h, and dried by blowing nitrogen gas.

The mineralization of HA followed the procedure we reported previously.[34] The GO and GO-Car substrates were incubated in the 1.5 × SBF (pH 7.4) solution in a six-well plate at 37 °C for 3, 7, and 14 days. After thoroughly washing with water several times, the product was dried under a vacuum and used for further analysis.

Characterization. Fourier transform infrared measurements were done on a Thermo Mattson FTIR. Scanning electron microscope (SEM) microscopy and energy dispersive X-ray spectrometer (EDX) was obtained on a Hitachi S-4800 field emission scanning electron microscope. The crystal phase was determined by X-ray diffraction (XRD) analysis using D/max-2400pc (Rigaku, Japan) with Cu-Ka radiation (λ = 1.54178 Å). All pH measurements were made with a pH-10C digital pH meter. The hydrophilicity was investigated using contact angle measurements. A ultrasonic cleaner was used to disperse the sample (KQ5200, China).

Cell Culture and Seeding. MC3T3-E1 cells were cultured in high-glucose DMEM supplemented with 10% FBS as well as antibiotic antimycotic solution containing 100 U mL^{-1} penicillin and 100 U mL^{-1} streptomycin sulfate. The culture conditions were a humidified atmosphere of 5% CO_2, 95% air at 37 °C.

For cell seeding, the dried glass, GO, and GO-Car substrates were placed in a 12-well plate. Prior to seeding with cells, the samples were sterilized under Co 60 (γ) laser for 6h.

Cell Proliferation. Cell proliferation was evaluated using the MTT assay. Basically, 5 × 10^4 cells were seeded on each film in 12-well tissue culture plates. MC3T3-E1 cell proliferation was assessed by 3-[4, 5-dimethylthiazol-2-yl]-2, 5-diphenyltetrazolium bromide (MTT) after 1, 3, and 7 days of cell culture. Culture medium was aspirated at the predetermined time point and the cell-sunbstrtes was washed with PBS and put into another 12-well plate; 900 μL of culture medium and 100 μL of MTT solution were added. This cultivation was allowed to last for 4h, after that 1 mL of 10% SDS-HCl was added and cultured overnight. Then, 100 μL of the solution was added to a 96-well plate for the absorbance measurement at 570 nm using a microplate reader. Three samples were tested for each incubation period, five parallel replicates (n = 5) for each sample were used to assess cell proliferation, and the maximum and minimum were deleted. Culture medium without cells was used as the blank test.

Cell Adhesion and Morphology. For the confocal microscopy image analysis, MC3T3-E1 cells were plated at a density of 5 × 10^4 in 12-well plates and grown on the coverslips. After incubation at 37 °C and in 5% CO_2 atmosphere for 1, 3, and 7 days, cells were fixed in 4%

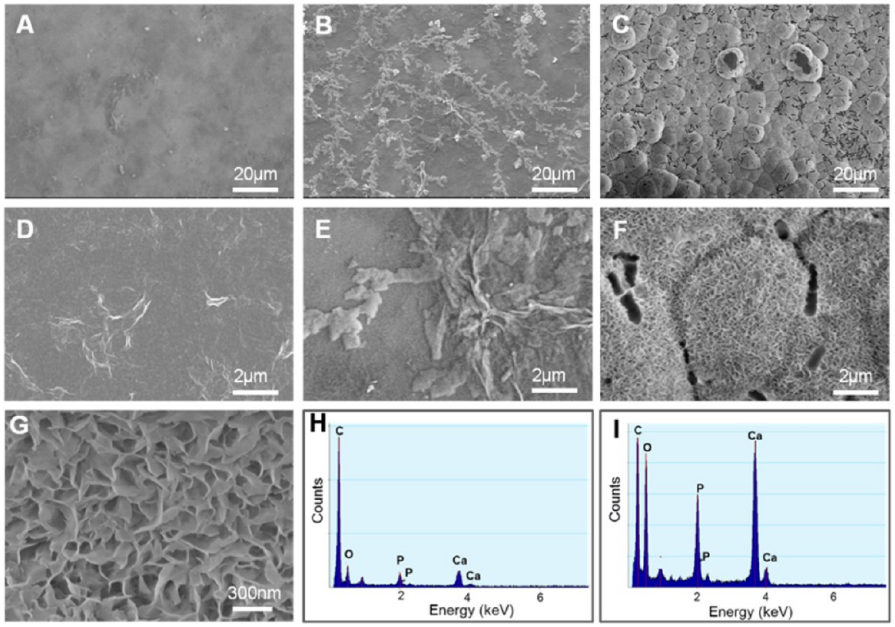

Figure 2. SEM images of GO-Car after (A, D) 0, (B, E) 7, and (C, F, G) 14 days mineralization. EDX of the mineral deposits on GO-Car after (H) 7 and (I) 14 days.

paraformaldehyde (Sigma-Aldrich), stained with acridine orange (Genview, USA) for 30 min and were washed with PBS for three times to remove free dyes. All confocal images were collected with a Zeiss Leica inverted epifluorescence/reflectance laser scanning confocal microscopy (LSCM, LEICA TCS SP2). The image was quantified using the analysis software (Leica Confocal Software). Five cells of each image were randomly selected to calculate the cell areas and the average value was quantified.

For the SEM observation, a density of 2×10^4 cells were seeded on each film in 12-well tissue culture plates. Cell morphology after 3 and 7 days of culture was observed by SEM (JSM-6380LV, Japan). Cell-substrates were washed with PBS and then fixed with 3% glutaraldehyde at 4 °C for 4h. The constructs were then dehydrated in a graded series of ethanol solutions (50, 70, 80, 90, and 100%) and dried under a vacuum. Afterward, the constructs were sputter coated with gold and examined using SEM at an accelerating voltage of 30 kV.

ALP Activity. For the ALP assay, 2×10^4 cells were seeded on the different substrate in a 24-well plate. The medium was changed every other day. ALP activity was evaluated using the cAKP stain kit (Jiancheng Co. Nanjing) after 1, 3, and 7 days of cell seeding. The assay was performed according to the manufacturer's instructions. First, cells on different films were fixed with the fixing solution for 3 min. Second, the substrate solution was added and then covered by a hydrophobic membrane for 15 min. Finally, cells were stained with hematoxylin for about 3 min, rinsed, and the images were collected with an AX80 system microscope.

Osteogenic Differentiation. MC3T3-E1 cells were seeded at 2×10^4 cells per well. An osteogenic medium, which consisted of complete medium supplemented with 0.2 mM ascorbic acid and 10 mM β-glycerol phosphate, was added after 24 h of cell seeding. The medium was changed every three days. After 14 days of induction, cell-film constructs were washed with PBS and fixed with 3% glutaraldehyde at 4 °C for 4 h. The constructs were then dehydrated and examined using SEM, following the same procedure as mentioned in the cell adhesion part.

3. RESULTS AND DISCUSSION

The surface modification of GO by carrageenan was first demonstrated by FTIR (Figure 1 and Figure S1 in the Supporting Information). The FTIR spectrum of GO-Car composite exhibits typical peaks of GO and carrageenan. The peak at 1258 cm^{-1} was assigned to vibration of S═O of sulfate esters, whereas the peaks at 931 and 846 cm^{-1} were assigned to the C−O vibration of 3,6-anhydro-D-glactose and the C−O−S of axial secondary sulfate of glactose,[35] respectively, confirmed the modification of GO by carrageenan. Biomimetic mineralization was induced by incubating each substrate in 1.5 × SBF solution.[36] The mineralized HA on the GO and GO-Car substrates was also monitored by FITR. After 7 days incubation, there was no typical peaks of HA observed from the GO substrate (Figure 1A). For the GO-Car, weak PO_4^{3-} bands appeared at 610, 562, 962, and 1035 cm^{-1} (Figure 1B), which are due to the bending, stretching, and vibration mode of PO_4^{3-}.[37,34] After 14 days, these peaks exhibit a much stronger intensity. However, there is no peak observed from the GO substrate. Note that carrageenan probably promoted the formation of the HA.

SEM were utilized to analysis the morphology and micro-structure of the substrates after mineralization. Figure 2A-C shows the minerals deposited on the surface of GO-Car after mineralization for 0, 7, and 14 days. SEM micrographs show minerals decorating a network after incubation for 7 days (Figure 2B). At higher magnification, it can be seen that the precipitate is composed of small irregular aggregates (Figure 2E). In the samples taken after 14 days of mineralization, the GO-Car surface was uniformly covered with spherical aggregated minerals with an average size of approximately 10 μm (Figure 2C). It can be clearly seen that the obtained mineral composite shown a macroporous structure with three-dimensional (3D) interconnected channels (Figure 2G). However, there was no HA minerals observed on the GO substrate after 14 days mineralization (see Figure S2 in the Supporting Information). The enhanced mineralization may be a result of the carrageenan modification. This can be explained by the fact that carrageenan has a very high negative charge density due to the presence of sulfonate groups ($-OSO^{3-}$), which enabled efficient interaction with calcium ions and other mineral ions present in the 1.5 × SBF solution and highly accelerated the nucleation of HA minerals.

The chemical composition of the mineral on GO-Car was further analyzed by EDX. As shown in Figure 2H and I, after 7

dx.doi.org/10.1021/am4057826 | ACS Appl. Mater. Interfaces 2014, 6, 3132−3140

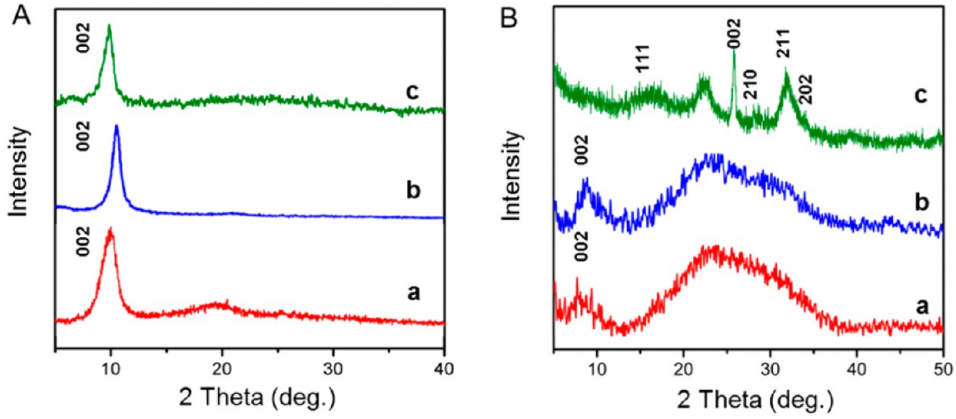

Figure 3. XRD patterns showing the phase of the (A) GO and (B) GO-Car (a) before and (b, c) after (b) 7 and (c) 14 days mineralization.

days incubation, only a minute amount of calcium and phosphorus were observed. However, significant calcium and phosphorus peaks were observed after 14 days, which can be attributed to the contribution from the HA. The molar ratio of Ca/P of the composite is 1.53, which is consistent with the biological apatites.[38]

XRD was used to monitor the structural phase of the deposited minerals (Figure 3). The peak at around 2θ = 9.9° of GO corresponds to the (002) reflection. There was no new peak observed after incubation. The peaks for GO-Car were observed at around 2θ = 9.9° corresponding to the (002) reflection. The broad peak at 20−30° indicated the modification of GO by carrageenan. For the samples after 7 days incubation, weak peaks were observed at 25.0 and 32.0°, suggesting a slight mineralization. The diffraction patterns of GO-Car after 14 days incubation show characteristic peaks at and 25.9 and 31.6°, correspond to the (002) and (211) reflection of HA hexagonal phase (JCPDS card, 09−0432). The broadened peaks compared to well-crystallized HA are probably due to the small particle size of the HA,[39,40] which is also confirmed by SEM observation.

The biocompatibility of the GO and GO-Car substrate was assessed by the MTT assay. We plated MC3T3-E1 cells on the three films. As shown in Figure 4, due to the low density of cells,

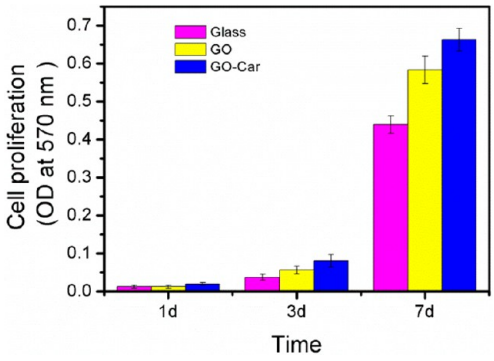

Figure 4. Proliferation of cells cultured on glass, GO, and GO-Car for 1, 3, and 7 days.

the optical density (OD) of the three different substrates is very low. On the third day, the GO-Car films exhibited greater cell growth than that of GO and glass films. This trend was verified over time after 7 days, which indicates that the GO based materials exhibit no cytotoxicity.

To further determine the effect of GO and GO-Car on the cell proliferation and morphology, MC3T3-E1 cells after incubated on the three kinds of substrates were evaluated by LSCM (Figure 5). The fluorescent images revealed similar density of cells on the GO, GO-Car, and glass after 1 day incubation. At day 3, there was a higher density of cells on GO-Car than other two. This difference was amplified after 7 days of culture, as the density of cells on GO-Car was markedly higher than that of the other two substrates. The nuclear fluorescence intensity of cells on GO-Car was also stronger than that on GO and glass, suggesting a much higher viability and proliferation of MC3T3-E1 cells.

Several parameters related to cell proliferation and morphology, including fluorescent intensity of nuclear (FIN), fluorescent intensity of cytoplasm (FIC), and cell area, were quantitatively analyzed. The FIN and FIC reflect the density and proliferation of cells. As shown in Panels A and B in Figure 6, at day 1, the FIN of cells equalized between the nanomaterial and the glass substrates. At days 3 and 7, the FIN of cells cultured on GO-Car substrate was distinctively higher than the other two substrates. The FIC of cells followed the same trend during the culturing. However, the difference is less marked. To quantify and compare cell proliferation ability, the nuclear ratio index (NRI) was calculated as the ratio between the FIN and FIC. As shown in Figure 6C, cells on GO-Car exhibited the highest proliferation ability compared to GO and glass. The NRI on GO is even lower than on glass, indicating that the function of carrageenan on GO probably promoted the cell-extracellular matrix (ECM) interactions and thus resulted an increased proliferation. To compare cell attachment, the area of cells was calculated by the average value of five cells selected randomly. At day 1, the cell area was tended to be broader on GO-Car and GO substrates compared with the glass substrates (Figure 6D). At day 3, the cell area equalized between GO and GO-Car. At day 7, the cell area on GO-Car is broader than the other two substrates. The cells exhibited better adhesion with the GO based nanomaterial than for bare glass. The cell adhesion and proliferation assay indicated that the prepared substrates show a very good biocompatibility. It is reported that the cell behavior can be also influenced by the wettability and hydrophilicity of the surface.[41] In this study, the hydrophobicity of the different substrates are measured as water contact angles, 58.6, 51.3, and 52.1° for glass, GO, and GO-Car, respectively (see Figure S3 in the Supporting Information), the similar hydrophilicity did not induce large differences in cell proliferation.

The cell morphology on different substrates after 3 and 7 days of culture was further observed by SEM (Figure 7). At day 3, the

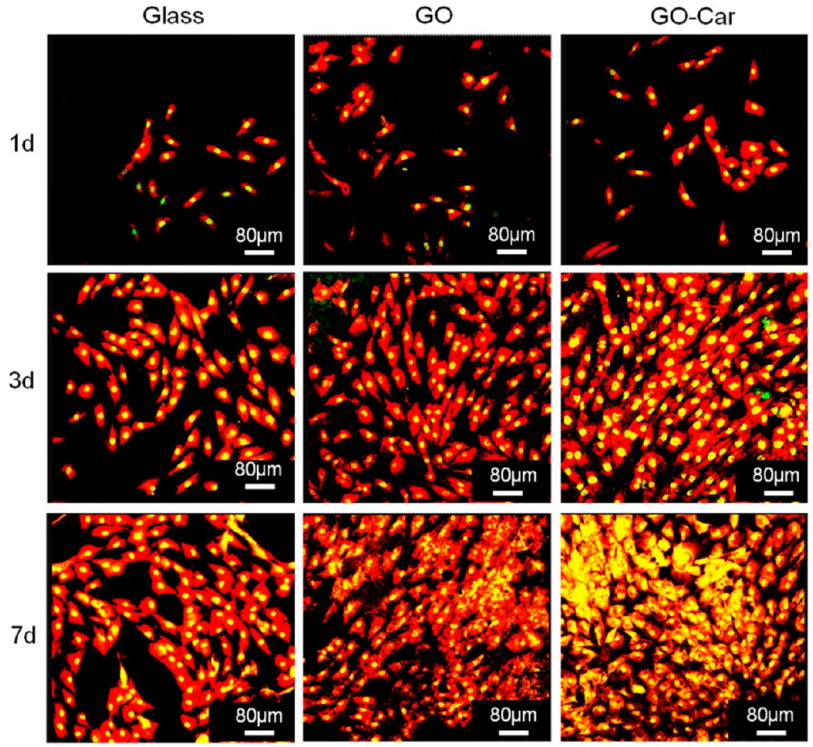

Figure 5. Confocal fluorescent images of MC3T3-E1 cells cultured on glass, GO, and GO-Car for 1, 3, and 7 days.

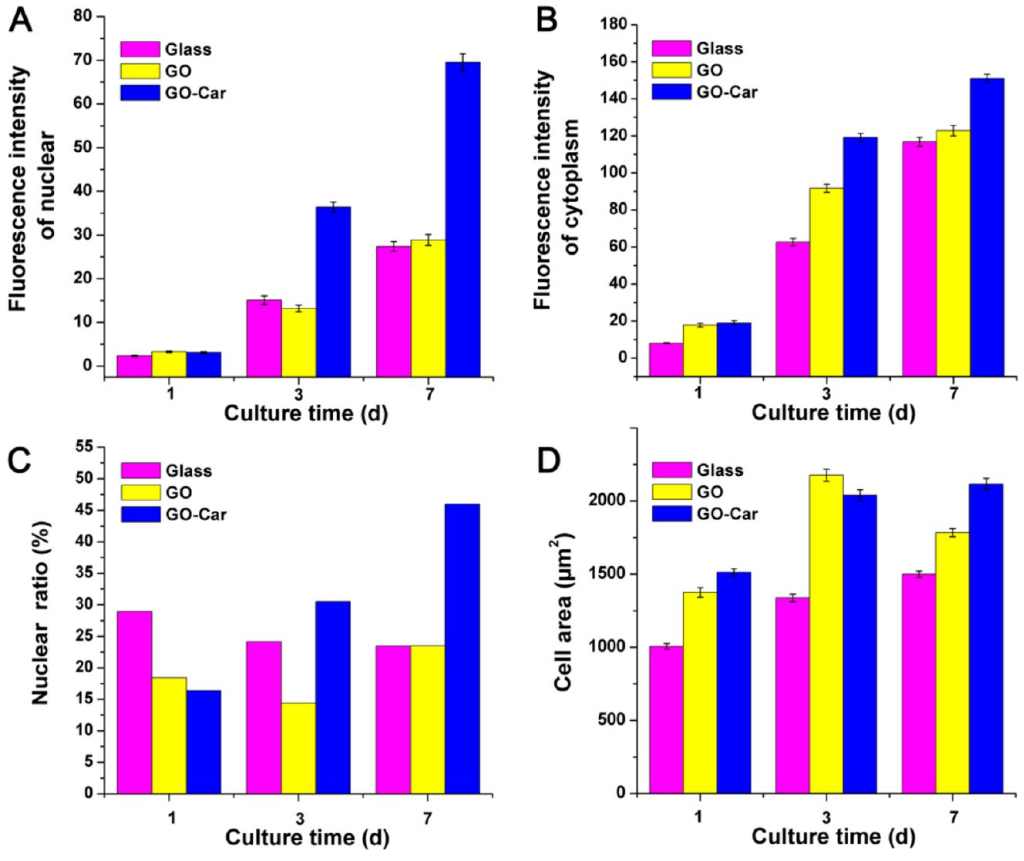

Figure 6. Quantitative analysis of cell adherence to the glass, GO, and GO-Car: (A) fluorescent intensity of nuclear, (B) fluorescent intensity of cytoplasm, (C) nuclear ratio index, and (D) cell area.

MC3T3-E1 cells presented a round shape on glass, but were elongated on GO and GO-Car substrates. The morphology of MC3T3-E1 cells exhibits a notable change after culturing for 7 days. Cells were homogenously dispersed on the on GO and GO-

dx.doi.org/10.1021/am4057826 | ACS Appl. Mater. Interfaces 2014, 6, 3132−3140

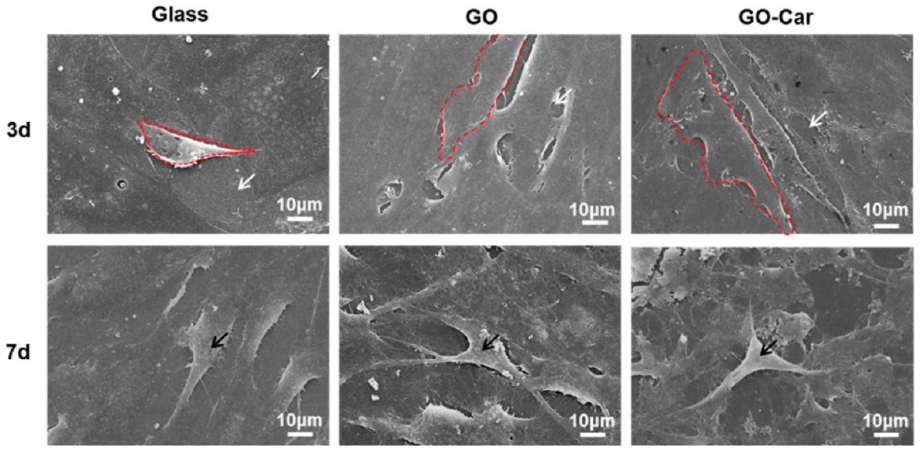

Figure 7. SEM images of MC3T3-E1 cells cultured on glass, GO, and GO-Car for 3 days (white arrows indicate the substrate and red dash boxed portion indicate morphology of cells) and 7 days (Black arrows indicate cells).

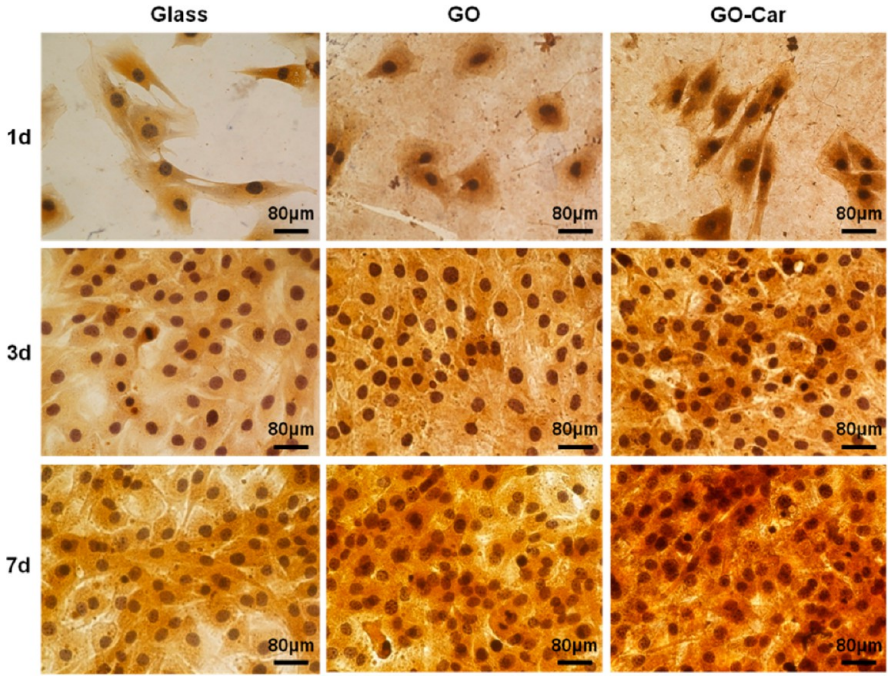

Figure 8. ALP stain images of MC3T3-E1 cells cultured on glass, GO, and GO-Car for 1, 3, and 7 days.

Car films surface and showed spindle-shape morphology with many filopodia extensions, whereas those on glass distributed sporadically. In addition, cells cultivated on GO-Car films were spread and appeared confluent, proving a better cell attachment. This phenomenon indicates that the biological assistance of carrageenan induced the viable cell attachment and proliferation.

As is well-known, markers correlated with the osteoblastic phenotype include: high ALP levels, expression of collagen I and noncollage-nous proteins, and finally the presence of bone apatite.[42−45] ALP is an early osteoblastic differentiation marker[46] and showing a mineralized extracellular matrix.[47] ALP activity was observed to measure influences of GO-Car on the osteogenic differentiation of MC3T3-E1 cells. As shown in Figure 8, there are numerous brown particles inside the cells after 3 days of culture, which represent the ALP activity points. At day 7, a significantly greater ALP activity was observed at GO-Car comparing to the GO and glass films. Moreover, it was noticed that there was a higher cell density on the GO-Car films. This result is also in good agreement with previous cell viability and proliferation assays. The ALP activity was further quantified. In the presence of ALP, *p*-NPP is transformed to *p*-nitrophenol and inorganic phosphate.[48] So the ALP activity can be determined by measuring the concentration of the *p*-nitrophenol product. As shown in Figure S4 in the Supporting Information, the ALP activity on all scaffolds increases remarkably with culture time during the 7 day culture period. After 3 and 7 days of incubation, cells on GO-Car showed higher levels of ALP activity than that on the GO and glass. This may be due to the fact that biocompatible carrageenan provided a more effective substrate for cellular proliferation and differentiation. Another possibility is that the improved nucleation of HA by carrageenan also resulted an enhanced differentiation of MC3T3-E1 cells.

To observe the stimulate-guided growth and mineralization of cells on GO-based interfaces, we acquired SEM images after 14 days of incubation. As shown in Figure 9A, the MC3T3-E1 cells sporadically covered the surface of the glass substrate. However,

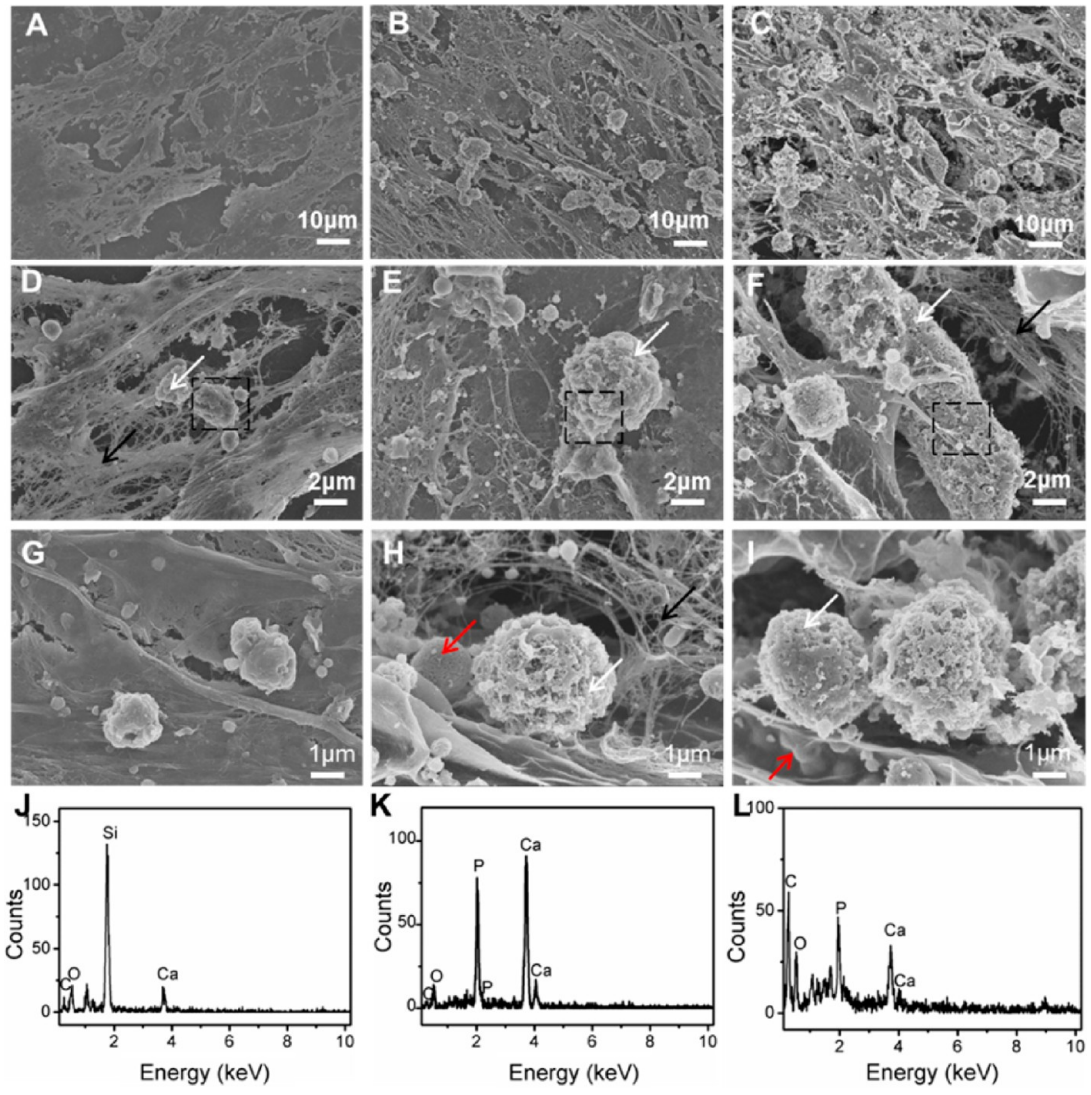

Figure 9. SEM images of MC3T3-E1 cells cultured on (A, D, G) glass, (B, E, H) GO, and (C, F, I) GO-Car for 14 days. EDX of the mineral deposits on (J) glass, (K) GO, and (L) GO-Car, which were obtained from the boxed portion of the micrograph. White, black, and red arrows indicate minerals, collagen, and vesicles, respectively.

Scheme 1. MC3T3-E1 Cell-Mediated Mineralization of HA on GO-Car Substrate

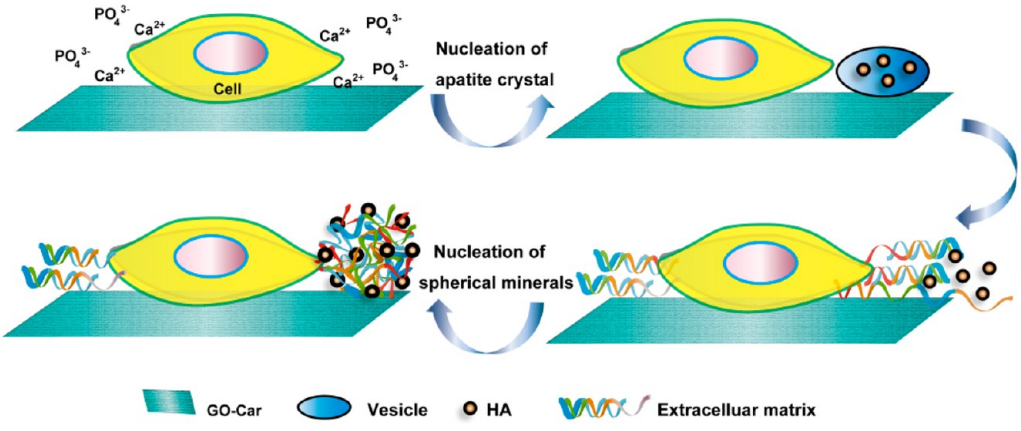

cells were well coated on the GO and GO-Car (Figure 9B, C). For the GO-Car substrates, cells were also observed to span across with each other, which suggested that the highly roughened and hydrophilic surface of GO-Car provided a more compatible structure for cell proliferation. The magnified image showed the presence of small spherical minerals located near the cells on the glass (Figure 9D), whereas the GO and GO-Car substrates were covered by a complex of fibrous organic

dx.doi.org/10.1021/am4057826 | *ACS Appl. Mater. Interfaces* 2014, 6, 3132−3140

bundles and embedded calcium phosphate (Figure 9E, F). Some mineralized matrix on the GO-Car substrates was even 20 μm in length (white arrow indicated in Figure 9F). Figures 9H, I show that the mineral deposits consisted of collagen fibers and some matrix vesicles, which were loaded with calcium phosphate crystals, while little mineral was observed on the glass substrates, without collagen fibers or matrix vesicles (Figure 9G). More images were shown in Figure S5 in the Supporting Information to indicate the cells, HA, collagen, and vesicles. It is known that biomineral nucleation and growth requires a local environment with sufficient supersaturation in the mineral precursors.[49] In our study, the GO-Car surface with sulfate groups facilitated the binding of calcium and thus served as nucleation points for HA. On the basis of these results, a scheme has been presented to describe the mineralization process. As illustrated in Scheme 1, the carrageenan surface facilitated the attachment of cells and the nucleation of HA. HA first nucleated within the vesicles, which are formed and released from the outer membranes of osteoblasts and related cells.[50] As the crystallite grows bigger, the HA crystal breaks through the vesicle and is exposed to the extracellular fluid and then is effectively encapsulated within a coherent coating of extracellular matrix, which resulted in individual spherical minerals consisting of calcium phosphate and collagen fibers. These spherical minerals underwent further nucleation on this surface and result in the growth or agglomeration of large bonelike tissues.

In addition, the composition of the mineral was characterized from the cell surface of the glass and material-coated substrates. As shown in the EDS results (Figure 9J, K, and L), the Ca and P contents for the GO-Car film were markedly higher than the GO film. The signals were incredibly low for the glass. The extent of mineralization of cells was also assessed via alizarin red S staining. Ca^{2+} quantitation assay results are illustrated in Figure S6 in the Supporting Information. Mineralized matrix was demonstrated by red-positive nodules above the cell. The calcium deposition of the GO-Car was higher than that of the pure GO and glass. From these results, we can estimate that the high cell proliferation and mineralization have been a result of carrageenan.

CONCLUSION

In summary, we designed a biointerface that promoted the mineralizaion both in simulated physiological condition and cell-mediated condition. GO-Car composites exhibited very good bioactivity and accelerated the nucleation of HA. We further investigated the mineralization of the GO-Car nanocomposite in the presence of MC3T3-E1 cells. The hybrid material exhibited good cellular activities including cell attachment, cell proliferation, and calcium deposition, which suggested that it is a promising substrate for induced synthesis of biomaterials in bone tissue regeneration and implantation. Further application of this hybrid material in bone tissue engineering is being explored in our laboratory.

ASSOCIATED CONTENT

Supporting Information

FTIR, water contact angles measurements, quantitative analysis of the ALP activity, and alizarin red S staining of mineral. This material is available free of charge via the Internet at http://pubs.acs.org.

AUTHOR INFORMATION

Corresponding Authors

*E-mail: xipx@lzu.edu.cn. Tel: +86 931 8912589; Fax: +86 931 8912582.
*E-mail: zengzhzh@lzu.edu.cn.

Notes

The authors declare no competing financial interest.

ACKNOWLEDGMENTS

This work was supported by the National Natural Scientific Foundation of China (21201092), the Research Fund for the Doctoral Program of Higher Education (20120211120020), the Gansu NST (1208RJYA028), and the Fundamental Research Funds for the Central Universities (Lzujbky-2012-213, Lzujbky-2012-65, and lzujbky-2012-189).

REFERENCES

(1) Yeo, M.; Jung, W. K.; Kim, G. Fabrication, Characterisation and Biological Activity of Phlorotannin-Conjugated PCL/b-TCP Composite Scaffolds for Bone Tissue Regeneration. *J. Mater. Chem.* **2012**, *22*, 3568−3577.
(2) Balakrishnan, B.; Banerjee, R. Biopolymer-Based Hydrogels for Cartilage Tissue Engineering. *Chem. Rev.* **2011**, *111*, 4453−4474.
(3) Lee, K. Y.; Mooney, D. J. Hydrogels for Tissue Engineering. *Chem. Rev.* **2001**, *101*, 1869−1880.
(4) Jeffrey, A. H.; Robert, L. Tissue Engineering. *Chem. Eng. News.* **1995**, *73*, 42−54.
(5) Mosiewicz, K. A.; Johnsson, K.; Lutolf, M. P. Phosphopantetheinyl Transferase-Catalyzed Formation of Bioactive Hydrogels for Tissue Engineering. *J. Am. Chem. Soc.* **2010**, *132*, 5972−5974.
(6) Nukavarapu, S. P.; Kumbar, S. G.; Brown, J. L.; Krogman, N. R.; Weikel, A. L.; Hindenlang, M. D.; Nair, L. S.; Allcock, H. R.; Laurencin, C. T. Polyphosphazene/Nano-Hydroxyapatite Composite Microsphere Scaffolds for Bone Tissue Engineering. *Biomacromolecules* **2008**, *9*, 1818−1825.
(7) Morozowich, N. L.; Nichol, J. L.; Allcock, H. R. Investigation of Apatite Mineralization on Antioxidant Polyphosphazenes for Bone Tissue Engineering. *Chem. Mater.* **2012**, *24*, 3500−3509.
(8) Sautier, J. M.; Nefussi, J. R.; Forest, N. Ultrastructural Study of Bone Formation on Synthetic Hydroxyapatite in Osteoblast Cultures. *Cells Mater.* **1991**, *1*, 209−217.
(9) Jarcho, M. Calcium Phosphate Ceramics as Hard Tissue Prosthetics. *Clin. Orthop. Relat. Res.* **1981**, *157*, 259−269.
(10) Bonfield, W.; Grynpas, M. D.; Tully, A. E.; Bowman, J.; Abram, J. Hydroxyapatite Reinforced Polyethylene−a Mechanically Compatible Implant Material for Bone Replacement. *Biomaterials* **1981**, *2*, 185−186.
(11) Malik, M. A.; Puleo, D. A.; Bizios, R.; Doremus, R. H. Osteoblasts on Hydroxyapatite, Alumina and Bone Surfaces in vitro: Morphology During the First 2 h of Attachement. *Biomaterials* **1992**, *13*, 123−128.
(12) Suchanek, W.; Yoshimura, M. Processing and Properties of Hydroxyapatite-based Biomaterials for Use as Hard Tissue Replacement Implants. *J. Mater. Res.* **1998**, *13*, 94−117.
(13) Kim, H. M; Miyaji, F.; Kokubo, T.; Nakamura, T. J. Preparation of Bioactive Ti and Its Alloys via Simple Chemical Surface Treatment. *J. Biomed. Mater. Res.* **1996**, *32*, 409−417.
(14) Zheng, X.; Huang, M.; Ding, C. Bond Strength of Plasma-sprayed Hydroxyapatite/Ti Composite Coatings. *Biomaterials* **2000**, *21*, 841−849.
(15) Alves, N. M.; Leonor, I. B.; Azevedo, H. S.; Reis, R. L.; Mano, J. F. Designing Biomaterials Based on Biomineralization of Bone. *J. Mater. Chem.* **2010**, *20*, 2911−2921.
(16) Liao, S. S.; Cui, F. Z.; Zhu, Y. J. Osteoblasts Adherence and Migration through Three-dimensional Porous Mineralized Collagen Based Composite: nHAC/PLA. *Bioact. Compat. Polym.* **2004**, *19*, 117−130.

(17) Chen, Y.; Bal, B. S.; Gorskis, J. P. Calcium and Collagen Binding Properties of Osteopontin, Bone sialoprotein, and Bone acidic Glycoprotein-75 from Bone. *J. Biol. Chem.* **1992**, *267*, 24871−24878.
(18) Hunter, G. K.; Goldberg, H. A. Modulation of Crystal Formation by Bone Phosphoproteins: Role of Glutamic Acid-rich Sequences in the Nucleation of Hydroxyapatite by Bone Sialoprotein. *Biochem. J.* **1994**, *302*, 175−179.
(19) Kosanovic, C.; Falini, G.; Kralj, D. Mineralization of Calcium Carbonates in Gelling Media. *Cryst Growth Des.* **2011**, *11*, 269−277.
(20) Chopin, T. The Red Alga Chondrus Crispus Stackhouse (Irish moss) and Carrageenans: a Review. *Can. Tech. Rep. Fish. Aquat. Sci.* **1986**, *1514*, l−69.
(21) Gomez-Navarro, C.; Burghard, M.; Kern, K. Ultralow Loading Pt Nanocatalysts Prepared by Atomic Layer Deposition on Carbon Aerogels. *Nano Lett.* **2008**, *8*, 2045−2049.
(22) Dikin, D. A.; Stankovich, S.; Zimney, E. J.; Piner, R. D.; Dommett, G. H. B.; Evmenenko, G.; Nguyen, S. T.; Ruoff, R. S. Preparation and Characterization of Graphene Oxide Paper. *Nature* **2007**, *448*, 457−460.
(23) Zhu, Y. W.; Murali, S.; Cai, W. W.; Li, X. S.; Suk, J. W.; Potts, J. R.; Ruoff, R. S. Graphene and Graphene Oxide: Synthesis, Properties, and Applications. *Adv. Mater.* **2010**, *22*, 3906−3924.
(24) Kim, F.; Cote, L. J.; Huang, J. Graphene Oxide: Surface Activity and Two-Dimensional Assembly. *Adv. Mater.* **2010**, *22*, 1954−1958.
(25) Chen, S.; Zhu, J. W.; Wu, X. D.; Han, Q. F.; Wang, X. Graphene Oxide-MnO_2 Nanocomposites for Supercapacitors. *ACS Nano* **2010**, *4*, 2822−2830.
(26) Suk, J. W.; Piner, R. D.; An, J.; Ruoff, R. S. Mechanical Properties of Monolayer Graphene Oxide. *ACS Nano* **2010**, *4*, 6557−6564.
(27) Liu, Z.; Robinson, J. T.; Sun, X.; Dai, H. PEGylated Nanographene Oxide for Delivery of Water-Insoluble Cancer Drugs. *J. Am. Chem. Soc.* **2008**, *130*, 10876−10877.
(28) Yang, X.; Tu, Y.; Li, L.; Shang, S.; Tao, X. Well-Dispersed Chitosan/Graphene Oxide Nanocomposites. *ACS Appl. Mater. Interfaces* **2010**, *2*, 1707−1713.
(29) Fan, H.; Wang, L.; Zhao, K.; Li, N.; Shi, Z.; Ge, Z. Fabrication, Mechanical Properties, and Biocompatibility of Graphene-Reinforced Chitosan Composites. *Biomacromolecules* **2010**, *11*, 2345−2351.
(30) Liang, J.; Huang, Y.; Zhang, L.; Wang, Y.; Ma, Y.; Guo, T.; Chen, Y. Molecular-Level Dispersion of Graphene into Poly(vinyl alcohol) and Effective Reinforcement of their Nanocomposites. *Adv. Funct. Mater.* **2009**, *19*, 2297−2302.
(31) Wan, C.; Frydrych, M.; Chen, B. Strong and Bioactive Gelatin−Graphene Oxide Nanocomposites. *Soft Matter.* **2011**, *7*, 6159−6166.
(32) Park, S.; An, J.; Piner, R. D.; Jung, I.; Yang, D.; Velamakanni, A.; Nguyen, S. T.; Ruoff, R. S. Aqueous Suspension and Characterization of Chemically Modified Graphene Sheets. *Chem. Mater.* **2008**, *20*, 6592−6594.
(33) Ryoo, S. R.; Kim, Y. K.; Kim, M. H.; Min, D. H. Behaviors of NIH-3T3 Fibroblasts on Graphene/Carbon Nanotubes: Proliferation, Focal Adhesion, and Gene Transfection Studies. *ACS Nano* **2010**, *4*, 6587−6598.
(34) Liu, H.; Xi, P.; Xie, G.; Shi, Y.; Hou, F.; Huang, L.; Chen, F.; Zeng, Z.; Shao, C.; Wang, J. Simultaneous Reduction and Surface Functionalization of Graphene Oxide for Hydroxyapatite Mineralization. *J. Phys. Chem. C* **2012**, *116*, 3334−3341.
(35) Thierry, C.; Ellen, W. A New and Rapid Method for Carrageenan Identification by FTIR Diffuse Reflectance Spectroscopy Drectly on Dried, Ground Algal Material. *Carbohydr. Res.* **1993**, *246*, 51−59.
(36) Kokubo, T.; Takadama, H. How Useful Is SBF in Pedicting In vivo Bone Bioactivity? *Biomaterials* **2006**, *27*, 2907−2915.
(37) Cao, H.; Zhang, L.; Zheng, H.; Wang, Z. Hydroxyapatite Nanocrystals for Biomedical Applications. *J. Phys. Chem. C* **2010**, *114*, 18352−18357.
(38) Jongpaiboonkit, L.; Franklin-Ford, T.; Murphy, W. L. Growth of Hydroxyapatite Coatings on Biodegradable Polymer Microspheres. *ACS Appl. Mater. Interfaces* **2009**, *1*, 1504−1511.
(39) Driessens, F. C.M.; Verbeeck, R. M. H. In *Biominerals*; CRC Press: Boca Raton, FL, 1990.
(40) Declercq, H. A.; Verbeeck, R. M. H.; De Ridder, Leo I.F.J.M.; Schacht, E. H.; Cornelissen, M. J. Calcification as an Indicator of Osteoinductive Capacity of Biomaterials in Osteoblastic Cell Cultures. *Biomaterials* **2005**, *25*, 4964−4974.
(41) Ponsonnet, L.; Reybier, K.; Jaffrezic, N.; Comte, V.; Lagneau, C.; Lissac, M.; Martelet, C. Relationship between Surface Properties (Roughness, Wettability) of Titanium and Titanium Alloys and Cell Behavior. *Mater. Sci. Eng., C* **2003**, *23*, 551−560.
(42) Laczka-Osyczka, A.; Laczka, M.; Kasugai, S.; Ohya, K. Behavior of Bone Marrow Cells Cultured on Three Different Coatings of Gel-derived Bioactive Glass−Ceramics at Early Stages of Cell Differentiation. *J. Biomed. Mater. Res.* **1998**, *42*, 433−442.
(43) Goto, T.; Kajiwara, H.; Yoshinari, M.; Fukuhara, E.; Kobayasi, S.; Tanaka, T. In vitro Assay of Mineralized-Tissue Formation on Titanium Using Fuorescent Staining with Calcein Blue. *Biomaterials* **2003**, *4*, 3885−3892.
(44) Andre-Frei, V.; Chevallay, B.; Orly, I.; Boudeulle, M.; Huc, A.; Herbage, D. Acellular Mineral Deposition in Collagen-Based Biomaterials Incubated in Cell Culture Media. *Calcif. Tissue Int.* **2000**, *66*, 204−211.
(45) Declercq, H.; Van den Vreken, N.; De Maeyer, E.; Verbeeck, R.; Schacht, E.; De Ridder, L.; Cornelissen, M. Isolation, Proliferation and Differentiation of Osteoblastic Cells to Study Cell/Biomaterial Interactions: Comparison of Different Isolation Techniques and Source. *Biomaterials* **2004**, *25*, 757−768.
(46) Gotoh, Y.; Hiraiwa, K.; Nagayama, M. In vitro Mineralization of Osteoblastic Cells Derived from Human Bone. *Bone Miner.* **1990**, *8*, 239−250.
(47) Stein, G. S.; Lian, J. B.; Owen, T. A. Relationship of Cell Growth to The Regulation of Tissue-Specific Gene Expression during Osteoblast Differentiation. *FASEB J.* **1990**, *4*, 3111−3123.
(48) Yeo, M. G.; Kim, G. H. Preparation and Characterization of 3D Composite Scaffolds Based on Rapid-Prototyped PCL/β-TCP Struts and Electrospun PCL Coated with Collagen and HA for Bone Regeneration. *Chem. Mater.* **2012**, *24*, 903−913.
(49) Weiner, S.; Dove, P. M. An Overview of Biomineralization Processes and the Problem of the Vital Effect. *Rev. Mineral. Geochem.* **2003**, *54*, 1−29.
(50) Anderson, H. C. Molecular Biology of Matrix Vesicles. *Clin. Orthop. Relat. Res.* **1995**, *314*, 266−280.